International Journal of Biological Macromolecules 260 (2024) 129368

Contents lists available at ScienceDirect

International Journal of Biological Macromolecules

journal homepage: www.elsevier.com/locate/ijbiomac

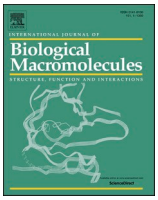

Highly deformable and strongly magnetic semi-interpenetrating hydrogels based on alginate or cellulose

Alberto Leon-Cecilla [a,b], Cristina Gila-Vilchez [a,b], Francisco J. Vazquez-Perez [a,b], Luis F. Capitan-Vallvey [c], Vanesa Martos [d,e], María D. Fernandez-Ramos [c], Luis Álvarez de Cienfuegos [b,f], Antonio L. Medina-Castillo [c,*], Modesto T. Lopez-Lopez [a,b,**]

[a] Universidad de Granada, Departamento de Física Aplicada, Campus de Fuentenueva, E-18071 Granada, Spain
[b] Instituto de Investigación Biosanitaria Ibs.GRANADA, E-18014 Granada, Spain
[c] Universidad de Granada, Departamento de Química Analítica, Campus de Fuentenueva, E-18071 Granada, Spain
[d] Universidad de Granada, Departamento de Fisiología Vegetal, Campus de Fuentenueva, E-18071 Granada, Spain
[e] Instituto de Biotecnología, Universidad de Granada, Campus de Fuentenueva, E-18071 Granada, Spain
[f] Universidad de Granada, Departamento de Química Orgánica, Unidad de Excelencia Química Aplicada a Biomedicina y Medioambiente, Campus de Fuentenueva, E-18071 Granada, Spain

ARTICLE INFO

Keywords:
Magnetic hydrogels
Carbohydrate biopolymers
Semi-interpenetrating polymer network

ABSTRACT

The effective implementation of many of the applications of magnetic hydrogels requires the development of innovative systems capable of withstanding a substantial load of magnetic particles to ensure exceptional responsiveness, without compromising their reliability and stability. To address this challenge, double-network hydrogels have emerged as a promising foundation, thanks to their extraordinary mechanical deformability and toughness. Here, we report a semi-interpenetrating polymer networks (SIPNs) approach to create diverse magnetic SIPNs hydrogels based on alginate or cellulose, exhibiting remarkable deformability under certain stresses. Achieving strong responsiveness to magnetic fields is a key objective, and this characteristic is realized by the incorporation of highly magnetic iron microparticles at moderately large concentrations into the polymer network. Remarkably, the SIPNs hydrogels developed in this research accommodate high loadings of magnetic particles without significantly compromising their physical properties. This feature is essential for their use in applications that demand robust responsiveness to applied magnetic fields and overall stability, such as a hydrogel luminescent oxygen sensor controlled by magnetic fields that we designed and tested as proof-of-concept. These findings underscore the potential and versatility of magnetic SIPNs hydrogels based on carbohydrate biopolymers as fundamental components in driving the progress of advanced hydrogels for diverse practical implementations.

1. Introduction

Smart materials capable of exhibiting changes in their mechanical and optical properties in response to external stimuli have received considerable attention [1,2] due to their great potential in the development of smart devices with remote actuation, such as guided catheters, artificial muscles, magnetic microvalves, multifunctional sensors, and biosensors, among others [3–6]. Magnetic hydrogels based on natural biopolymers constitute one of the most promising types of smart materials due to their unique combination of biocompatibility, flexibility, and responsiveness to magnetic fields [7,8], providing unique features such as precise remote actuation [9–13]. However, achieving a strong responsiveness to magnetic fields requires moderately high concentrations of magnetic particles in the hydrogel, that usually result in a loss of integrity of the polymer network or, at best, in substantial weakening of the mechanical properties and the stability of the resulting magnetic hydrogel [10,13–17]. This mechanical weakness in magnetic hydrogels confines their applicability mainly to areas that require limited low-level loading [18,19], whereas works that report the use of magnetic hydrogels based on biopolymers to applications that demand

* Corresponding author.
** Corresponding author: M.T. Lopez-Lopez, Universidad de Granada, Departamento de Física Aplicada, Campus de Fuentenueva, E-18071 Granada, Spain.
E-mail addresses: antonioluismedina@ugr.es (A.L. Medina-Castillo), modesto@ugr.es (M.T. Lopez-Lopez).

https://doi.org/10.1016/j.ijbiomac.2024.129368
Received 2 October 2023; Received in revised form 12 December 2023; Accepted 8 January 2024
Available online 12 January 2024

superior mechanical properties, such as soft actuators or artificial muscles, are scarce [20,21].

Strategies to overcome this limitation include a proper functionalization of the particle surface, so that the particles participate in the polymer network by covalent or ionic bonding [22,23] or to increase the concentration of polymer to strengthen the resulting network [24]. Unfortunately, the former usually requires complex and highly time-consuming protocols to functionalize the surface of the particles, which limit their practical application, and the latter results in decreased porosity that could have a negative impact in different applications, especially in the biomedical field.

Another promising approach to prepare magnetic hydrogels that combine strong responsiveness to applied magnetic fields and mechanical stability is based on the use of interpenetrating polymeric networks (IPNs) or semi-interpenetrating polymeric networks (SIPNs) [25–28]. IPNs are systems comprising two or more three-dimensional polymeric networks that are partially intertwined at the molecular scale but have no covalent bonding with each other, whereas in SIPNs the distinguishing feature is that the molecular scale penetration occurs between a three-dimensional polymeric network and a non-crosslinked linear or branched polymer [29]. Both IPNs and SIPNs combine different properties of the distinct constituent materials and have been considered a straightforward strategy to combine and tune the functional properties of polymeric materials [30–32]. Furthermore, double network hydrogels, a special type of IPNs hydrogels, are characterized by combining high water content with high mechanical compliance and toughness [33–37]. Due to their superior mechanical properties, these IPNs and SIPNs could withstand high concentrations of particles without substantial deterioration of their mechanical stability.

In this work, an approach based on the use of SIPNs consisting of a cross-linked network made of acrylamide and *N*,*N*′-methylenebisacrylamide and biopolymer consisting of any of five different natural carbohydrates (sodium alginate; 2-hydroxyethyl cellulose of two different molecular weights; carboxymethyl cellulose sodium salts of two different molecular weights) was used to prepare magnetic SIPNs (Mag-SIPNs) hydrogels with excellent stretchability (strains at break up to 220 % under tensile stress), high water content (up to 87.89 % w/w) [38] and strong responsiveness to applied magnetic fields (Fig. 1A). This last characteristic was achieved by embedding silica-coating iron microparticles at moderately high concentrations (up to 26.2 % w/w) in the polymer network, without substantial detriment of the excellent mechanical properties of the SIPNs, but with a reduction on their water concentration. The use of iron microparticles in this work is a differential feature with respect to most works in the field of magnetic IPNs or SIPNs hydrogels based mainly on magnetite nanoparticles [39–41], with only a few examples based on magnetic microparticles [42–44]. The use of strongly magnetic (e.g., iron) microparticles is also a requirement to achieve a stronger responsiveness to the magnetic fields. Furthermore, the performance, reliability, and stability of the Mag-SIPNs hydrogels were evaluated in a proof-of-concept application that demanded strong responsiveness to magnetic fields, specifically a hydrogel luminescent oxygen sensor controlled by a magnetic field. For this, we designed a disk-like hydrogel consisting of an inner non-magnetic circle containing O_2-sensitive luminescent nanoparticles, and an outer magnetic ring. It was thanks to the strong magnetic responsiveness of the Mag-SIPNs that the magnetic luminescent oxygen sensor could be firmly fixed inside the measurement cell from the outside, by a system of coaxial magnets placed around the optical fiber, allowing easy and reliable reading of the luminescent signal. This sensor solves one of the most limiting problems in the optical measure of O_2 in liquid systems, which is the lack of fixation of the sensor in the measurement cell, which prevents a reliable reading of the optical signal from the outside.

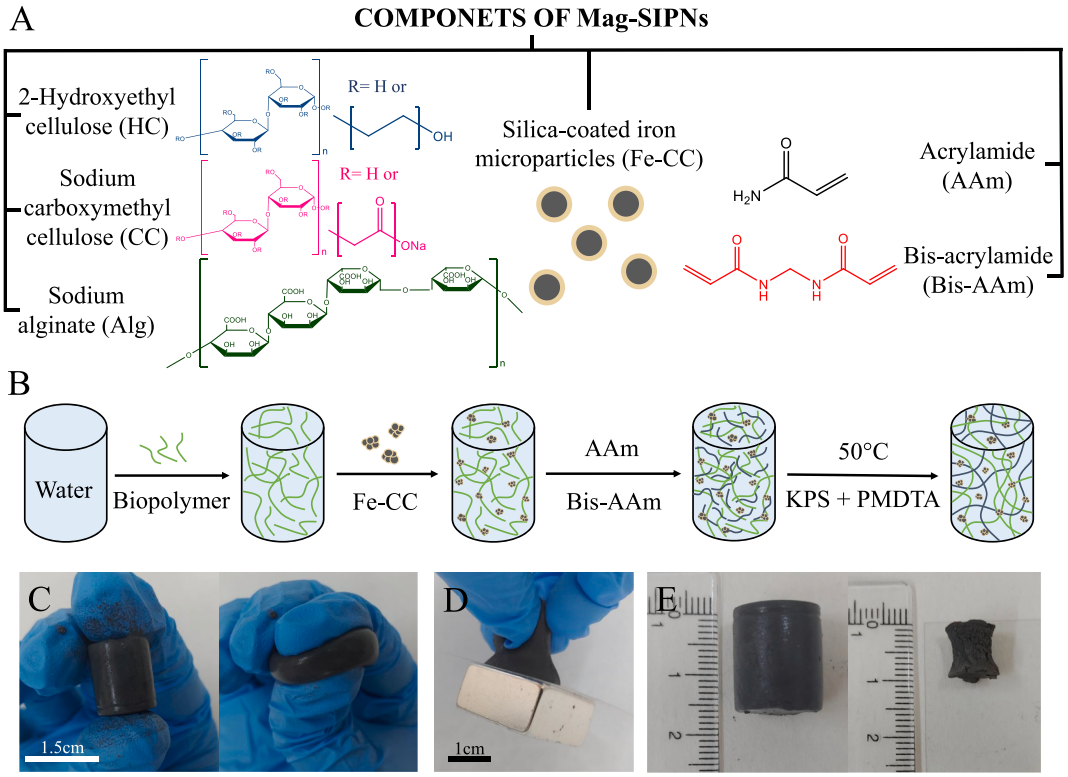

Fig. 1. (A) Chemical composition of Mag-SIPNs hydrogels. (B) Preparation protocol of the Mag-SIPNs hydrogels. (C) High deformability of Mag-SIPNs hydrogels. (D) Strong magnetic response of Mag-SIPNs hydrogels, which were able to hold a 25 × 25 × 13 mm NdFeB permanent magnet (~ 60 g). (E) Swollen (left) and dehydrated (right) Mag-SIPNs hydrogel with a 6.4 % w/w of Fe-CC -note that the initial content of water was 64.86 % w/w.

2. Material & methods

2.1. Materials

Acrylamide (AAm), *N*,*N*′-methylenebisacrylamide (Bis-AAm), 2-hydroxyethyl cellulose $M_v \sim$ 720,000 (HC720) (2 % w/w, 25 °C, water: 4500–6500 mPas; code 434973) and $M_v \sim$ 1,300,000 (HC1300) (1 % w/w, 25 °C, water: 3400–5000 mPas; code 434981), high viscosity carboxymethyl cellulose sodium salts (CChigh) (1 % w/w, 25 °C, water: 1500–3000 mPas; code C5013), medium viscosity carboxymethyl cellulose sodium salts (CCmedium,) (2 % w/w, 25 °C, water: 400–1000 mPas; code 21902), potassium peroxodisulfate (KPS), N,N,N′,N″,N″-pentamethyldiethylenetriamine (PMDTA), and platinum octaethylporphyrin (PtOEP; luminescent O_2 probe; $\lambda_{exc} = 380$ nm, $\lambda_{em} = 650$ nm) were purchased from Sigma Aldrich (USA). Medium viscosity sodium alginate (1 % w/w, 20 °C, water: 350–550 mPas; code A3249) was purchased from PanReac AppliChem ITW Reagents (Spain). The relative content of mannuronic to guluronic acid was experimentally estimated using protocols based on ellipsometry [45,46] (Fig.S-1). Both ellipsometric methods showed that the composition of this alginate is as it follows: Method of Donati et al. [45]: 18.7 % guluronic acid, 28.9 % mannuronic acid, and 52.4 % mixed sequences; Method of Morris et al. [46]: 17.1 % guluronic acid, 34.3 % mannuronic acid, and 48.7 % mixed sequences, which are in good agreement with the results of the method of Ref. [45]. Sodium lauryl sulfate (SDS) 95 % extra pure, chloroform ($CHCl_3$) stabilized with ethanol, and pellets of sodium hydroxide (NaOH) of reagent grade were purchased from Scharlau (Spain). Poly (styrene-*co*-maleic anhydride; 7 % maleic anhydride, $M_w = 80{,}000$ Da) was purchased from ARKEMA Sartomer® (France). Silica-coated iron powder (Fe-CC powder) was supplied by BASF (Germany). Fe-CC powder consisted of spherical micronsized particles of diameter 1.4 ± 0.6 μm, volumetric mass density of 7.71 ± 0.19 g cm^{-3}, and a typical ferromagnetic behavior with saturation magnetization $M_S = 1587 \pm 2$ kA/m. All reagents were used as received and all water solutions were prepared using milli-Q water.

2.2. Synthesis of the Mag-SIPN hydrogels

In Fig. 1B a diagram of the preparation protocol of the Mag-SIPNs is shown. First, 1.67 % w/w water solutions of sodium alginate (Alg), 2-hydroxyethyl cellulose (HC720 and HC1300), or carboxymethyl cellulose sodium salts (CChigh and CCmedium) were prepared separately. Subsequently, Fe-CC microparticles were added to the polymeric solutions, the resulting mixtures were sonicated for 15 min, followed by shaking (orbital rotator) until homogeneous suspensions were formed (1 h). Afterwards, Bis-AAm and AAm were dissolved in water. Then, the monomer (Bis-AAm/AAm) solution was mixed for 1 h under vigorous stirring with the suspensions of Fe-CC microparticles. Finally, an aqueous solution of thermal initiator KPS (10 mg/mL) and the accelerant (PMDTA) were added to the Bis-AAm/Aam/Fe-CC/biopolymer mixtures, and then, these mixtures were cured at 50 °C overnight. The concentrations of the compounds used were as it follows: 87.89 % w/w of milli-Q water, 0.89 % w/w of biopolymer, 0.13 % w/w of Bis-AAm, 11.02 % w/w of AAm, 0.07 % w/w of KPS, and 0.11 μmol/g of PMDTA (all these concentrations are given with respect to the total mixture without particles). The Fe-CC particle concentrations were 6.4, 12.0, 17.2, 21.9, and 26.2 % w/w (with respect to the total mass of hydrogel). The final water content in the hydrogels was calculated from these data. As an example, for a hydrogel containing 12.0 % w/w of Fe-CC, the final concentration of water was $(100 - 12) \times 87.89/100 = 77.3432\%w/w$ [47].

2.3. Characterization protocols

2.3.1. Characterization of the gelation kinetics

The gelation kinetics of the Mag-SIPNs hydrogels were investigated by subjecting the samples to oscillatory shear stress using a rotational rheometer (Bohlin CS-10), provided with a concentric cylinder geometry and at a constant temperature (50 ± 1 °C). For this aim, the polymerization mixtures Fe-CC/biopolymer/AAm/Bis-AAm/KPS/PMDTA were poured into the cylinder geometry of the rheometer, and the evolutions of the viscoelastic moduli were measured for an imposed oscillatory shear of constant frequency (1 Hz) and strain amplitude (0.3 %), within the linear viscoelastic region (LVR).

2.3.2. Characterization of the mechanical properties

The rheological properties under oscillatory shear of the hydrogels were determined at constant temperature (25 ± 1 °C) using a MCR300 Physica Anton-Paar rheometer equipped with a plate-plate geometry of 20 mm of diameter. The LVR of the different hydrogels was determined by subjecting them to strain amplitude sweep tests at a constant frequency of 1 Hz and stepwise increasing shear strain amplitude (γ), obtaining the values of the storage (G') and loss (G'') moduli versus γ. From the resulting curves, the characteristic values of G' and G'' corresponding to the LVR were calculated by averaging the total extension of the LVR. Afterward, the trends of G' and G'' versus frequency were obtained, by frequency sweep tests performed at constant shear strain amplitude ($\gamma_0 = 0.3$ %) within the LVR and increasing frequency from 0.1 to 10 Hz. The mechanical behavior of the hydrogels under tensile and compressive stress was determined at room temperature (25 °C) using a hybrid rheometer (Discovery HR-1, TA Instruments) and a universal testing machine (Instron 3345, Instron), respectively. Firstly, the samples were prepared in a mold with dog-bone shape for the characterization under tensile stress. Before placing the samples in the apparatus, their cross-sectional area was measured. Then, the samples were clamped in the geometry of the rheometer, which had a groove in its surface to prevent the sample from slipping. Once the hydrogels were firmly fixed in the clamps of the rheometer, a slight normal tensile axial force was applied (0.01 N) to reach a uniform starting condition for all the samples, and to ensure a homogeneous force transmission at the beginning. During the measurement the hydrogels were deformed at a constant rate of 50.0 μm/s until breakage. Then, from the engineering stress vs. strain curves, the tensile modulus and the tensile strain at break were obtained. The tensile modulus was calculated as the slope of the linear regression of strain versus tensile stress from a strain of 10 % to its breakage. The strain at break was obtained from the last point of the curves before the sample breakage. For measurements under compression, the materials were characterized using a plate-plate geometry with a rough surface to avoid the slipping of the samples. In this case, the hydrogels were prepared with cylindrical shape and before measurement, the diameter of their cross-sectional area was also determined. The measurement process was carried out in the same conditions as the tensile characterization, with the difference in the direction of the force. The analysis of the results was similar to the tensile case, with the only difference that the compressive modulus was determined only for a strain below 20 %.

2.3.3. Scanning Electron Microscopy (SEM)

Samples were prepared by critical point drying, and then fractured to observe de internal structure. Finally, they were deposited on SEM supports and coated with a fine carbon layer. For SEM images and Energy-Dispersive X-ray spectroscopy (EDX) a Zeiss, AURIGA (FIB-FESEM) equipment was used.

2.3.4. Characterization of hydrogel swelling

The SIPNs hydrogels were immersed in milli-Q water and the evolution of their mass was recorded over time, by extracting them from the water and obtaining their weight using a microbalance.

2.3.5. Magnetic characterization

Magnetization curves of the iron microparticles (Fe-CC) and the different Mag-SIPNs hydrogels were measured using a magnetometer

SQUID QUANTUM DESIGN MPMS XL.

2.3.6. Magnetic field-induced contraction of the Mag-SIPNs hydrogels

Mag-SIPNs hydrogels of 5 × 5 × 20 mm were cured as described above in adequate molds of rectangular shape. Afterwards, the hydrogels were placed inside a reservoir of the same dimensions and a magnetic field was applied with a 25 × 25 × 13 mm NdFeB (N40) permanent magnet. This magnet produced a field gradient of 25.8 ± 0.4 mT/mm at 0–8 mm from its surface and of 8.0 ± 0.3 mT/mm at 12–20 mm from its surface (Fig. S-2). The contraction of each sample was videorecorded, and the linear contraction defined as the percentage of length change (ΔL) divided by the initial length (L_0) was analyzed using the open-source software Tracker.

2.4. Application as Magnetic Luminescent O_2 Sensor (ML-OSen)

The hydrogels that composed the oxygen sensor were prepared following the steps described above, using HC720 as biopolymer due to its appropriate mechanical properties and lower swelling capacity (see Sections 3.1.3 and 3.2). One change in the protocol was required to avoid the excessive swelling of this hydrogel: specifically increasing the concentration of the crosslinker agent Bis-AAm by a factor of four for the non-magnetic hydrogel, and by a factor of eight for the magnetic one. Since the sensor was composed of two different parts (magnetic part and non-magnetic sensor part), first a magnetic hydrogel with cylindrical shape containing Fe-CC particles at a concentration of 26.2 % w/w was prepared. Then, a concentric cylindrical hole of 8 mm of diameter was punctured in the magnetic hydrogel. Afterwards, a pre-hydrogel mixture substituting the magnetic particles by O_2-sensitive luminescent nanoparticles (Lu-NPs) at a concentration of 2.0 % w/w with respect to the total polymer mass was prepared. This mixture was poured in the hole previously punctured in the magnetic hydrogel and the system was cured at 50 °C overnight. After the curing was over, the cylindrical sample was cut into disks with a thickness of 2 mm, to ensure a smooth surface and a good coupling with the optical fiber.

The aforementioned Lu-NPs (99 ± 7 nm of diameter) were prepared by encapsulation of PtOEP into poly(styrene-*co*-maleic anhydride; 7 % maleic anhydride) by mini-emulsion solvent evaporation [47]. Firstly, a solution of SDS in water (0.3 mg/mL) and another one of poly(styrene-co-maleic anhydride; 7 % maleic anhydride) (105 mg/mL) and PtOEP (1.05 mg/mL) in chloroform were prepared. Both solutions were mixed in a proportion of 40:3, respectively. The biphasic mixture was cooled in an ice bath and sonicated with a high-energy probe sonicator (Branson S-450 Digital) at 50 % amplitude for five minutes to form a mini-emulsion. Then, the chloroform was evaporated within a few minutes under a nitrogen flow, and the maleic anhydride groups (7 %) of the Lu-NPs were hydrolyzed by addition of 2 mL of NaOH 0.5 M (Lu-Nps were kept under stirring in this basic media for at least 15 min). Finally, the Lu-NPs were centrifuged, washed with milli-Q water, and reconstituted in water at a concentration of 45 mg/mL.

2.5. Statistical analysis

For each set of experimental conditions, at least three different samples were measured. The mean value and standard error of each magnitude is provided in this manuscript. One-way and two-way Anova and Tukey *post-hoc* ($\alpha = 0.05$ in all cases) were used to statistically compare the mean values of the magnitude regarding the different experimental conditions such as the natural carbohydrate biopolymer used and the magnetic particles concentration. Detailed statistical comparisons are shown in Tables S-1 and S-2.

3. Results & discussion

3.1. Mechanical properties of Mag-SIPNs hydrogels

The SIPNs hydrogels (non-magnetic and magnetic) studied in this work were synthesized using acrylamide and *N,N′*-methylenebisacrylamide to form the cross-linked covalent network, along with five natural carbohydrate biopolymers (please refer to Section 2 and Table 1 for detailed information). The chemical composition of Mag-SIPNs is illustrated in Fig. 1 and their fabrication procedure is extensively described in Section 2.2.

3.1.1. Gelation kinetics of Alginate Mag-SIPNs

Firstly, the gelation kinetics of the SIPNs hydrogels were studied. The presence of magnetic microparticles was expected to significantly alter the kinetics. Furthermore, an extended gelation time could result in the sedimentation of the microparticles due to gravitational forces before reaching the gel point, leading to the formation of non-uniform magnetic hydrogels. Therefore, achieving a high gelation rate was crucial to obtain homogeneous and reproducible Mag-SIPNs. The gelation kinetics were investigated by using a Bohlin CS-10 rotational rheometer with a concentric cylinder geometry at a constant temperature of 50 ± 1 °C. The polymerization mixtures were poured into the cylinder geometry, and the gelling samples were subjected to oscillatory shear of constant low amplitude and frequency, monitoring the time evolution of the storage (G') and loss (G'') moduli (for more details, please refer to Section 2.3.1). The gelation kinetics of the Alginate Mag-SIPNs hydrogels were investigated in relation to the concentration of both iron microparticles and N,N,N′,N″,N″-pentamethyldiethylenetriamine (PMDTA; polymerization accelerant) [48]. Typical curves demonstrated an initial liquid state of the mixtures ($G' < G''$), followed by a sharp increase of both viscoelastic moduli and, finally, a plateau region with $G' > G''$, corresponding to well-formed hydrogels (Fig. 2A).

The gel point is usually determined as the point where G' consistently becomes higher than G'', although a more general method to detect the gel point is the Winter-Chambon criterion [49,50]. In this study, we identified the gel point as the point where a sharp increase in the viscoelastic moduli occurred since the crossover of G' and G'' was not observed in some cases, and this criterion yielded similar values to the crossover when applicable. We noticed a trend of the gelation time decreasing with an increase in the amount of the accelerant (PMDTA), while the addition of magnetic particles significantly increased the gelation time (Fig. 2B and C). Therefore, to maintain a fast-gelling process and prevent undesired particle settling, a larger amount of PMDTA was required as the particle content increased. However, depending on the molecular weight of the biopolymer a slight gradient in concentration of iron particles along the height of the hydrogel was unavoidable (refer to Section 3.2).

The accelerant did not seem to have a significant effect on the final mechanical properties of non-magnetic Alginate SIPNs hydrogels, as

Table 1
Natural carbohydrate biopolymers used to synthesize the different Mag-SIPNs with the name used along the manuscript and the different magnetic particle concentrations studied in each case.

Carbohydrate Biopolymer	Mag-SIPN Name	Magnetic Particle Concentration (% w/w)
Alginate (medium viscosity)	Alginate	6.4, 12.0, 17.2, 21.9, 26.2
Carboxymethyl cellulose sodium salt (medium viscosity)	CCmedium	6.4
Carboxymethyl cellulose sodium salt (high viscosity)	CChigh	6.4
2-hydroxyethyl cellulose (M_v ~ 720,000)	HC720	6.4
2-hydroxyethyl cellulose (M_v ~ 1,300,000)	HC1300	6.4

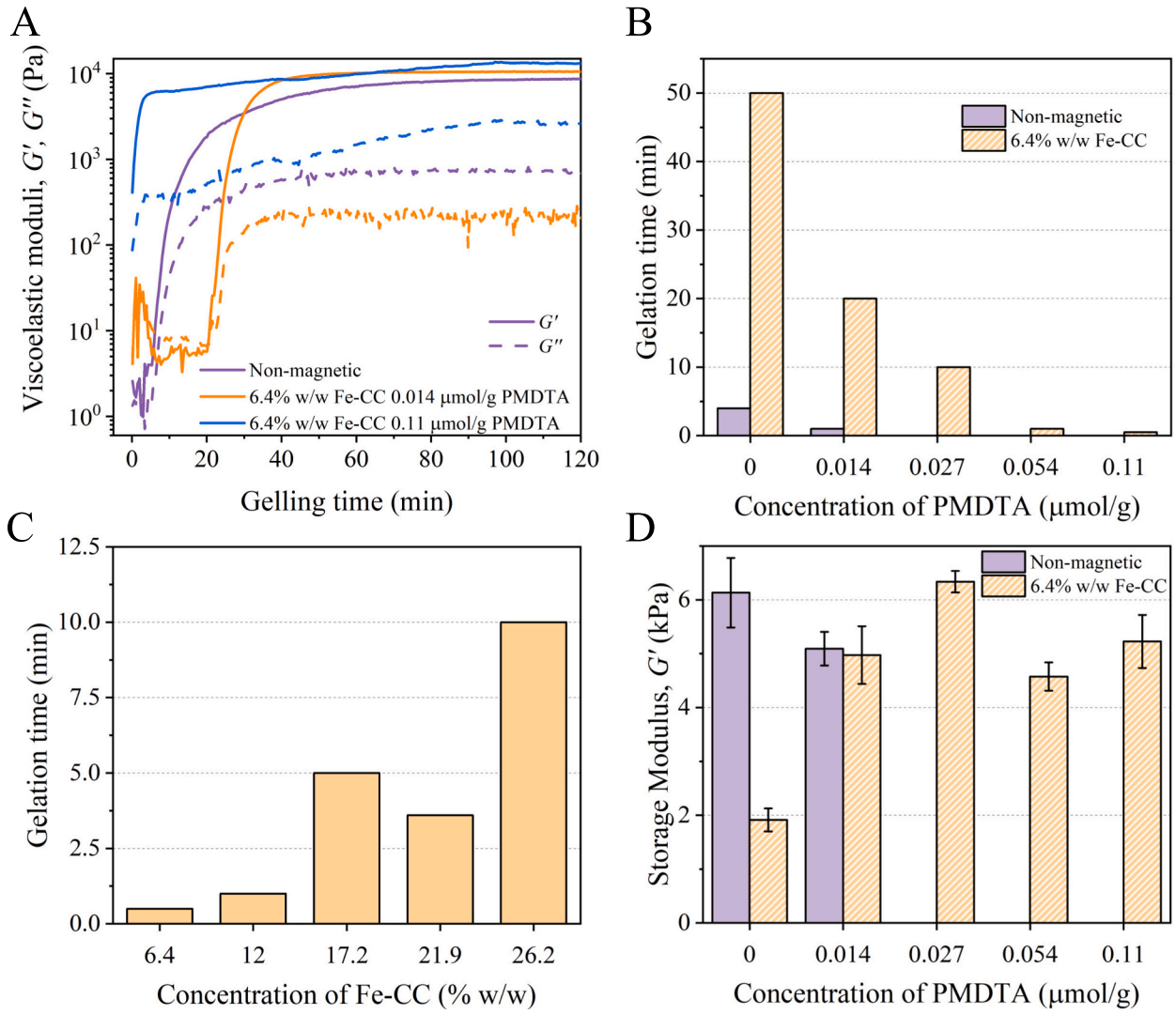

Fig. 2. Gelation kinetics (A) and gelation time (B) of Alginate Mag-SIPNs hydrogels at various concentrations of iron microparticles (Fe-CC) and accelerant (PMDTA). (C) Gelation time of Alginate Mag-SIPNs hydrogels as a function of the concentration of iron microparticles (with a fixed concentration of PMDTA: 0.11 µmol/g). (D) Steady-state value of the storage modulus within the linear viscoelastic region for several Alginate SIPNs hydrogels at different concentrations of PMDTA. Note that A, B and C only show one representative measurement for each experimental condition.

quantified by the values of *G'* (Fig. 2D). However, in the case of Mag-SIPNs, PMDTA did have a notable impact on the final mechanical properties, and a minimum concentration of PMDTA was required to achieve values of the storage modulus comparable to those of the non-magnetic SIPNs hydrogels. It should be noted that the value of *G'* decreased by a factor of 3 for hydrogels containing 6.4 % w/w of iron microparticles, with respect to non-magnetic hydrogels (Fig. 2D). One hypothesis for this behavior is that the gravitational settling of iron microparticles disrupted the polymerization process, requiring rapid gelation to prevent this undesired effect and obtaining well-formed magnetic hydrogels with optimal mechanical properties. Following this result, a concentration of PMDTA of 0.11 µmol/g was used in most cases in this work.

3.1.2. Mechanical characterization of Alginate Mag-SIPNs

A comprehensive characterization of the mechanical properties of fully gelled Alginate Mag-SIPNs hydrogels under different stresses (oscillatory shear stress, compressive stress, and tensile stress) was conducted. Strain amplitude sweeps (Fig.S-3A) demonstrated the typical behavior of a gel-like viscoelastic material, with a plateau-like region observed for small shear strain amplitudes where $G' > G''$. This plateau-like region defines the linear viscoelastic region (LVR). At higher strain amplitudes, the storage modulus decreased while the loss modulus initially sharply increased, followed by a subsequent decrease, within a region for which $G' < G''$, corresponding to the nonlinear viscoelastic region. This indicates a breakage of the internal structure of the material. Furthermore, the viscoelastic moduli were analyzed as a function of frequency for shear strain amplitude values within the LVR (Fig.S-3B). Once again, a typical gel-like behavior was observed, characterized by values of the viscoelastic moduli rather independent of frequency, with $G' > G''$.

The effect of incorporating magnetic particles into Alginate SIPNs hydrogels was also investigated. Fig. 3A and B present the average values of the viscoelastic moduli within the LVR for varying concentrations of iron microparticles ranging from 6.4 to 26.2 % w/w, with a fixed amount of accelerant. Consistent with the results of Fig. 2D, a decrease in the viscoelastic moduli values was observed as the magnetic particle content increased. While the decrease in *G'* was not statistically significant when adding up to 6.4 % w/w of magnetic particles compared to their non-magnetic counterpart, there was a statistically significant decrease in *G'* for hydrogels with 12.0 to 26.2 % w/w of magnetic particles. This indicates that the presence of magnetic particles

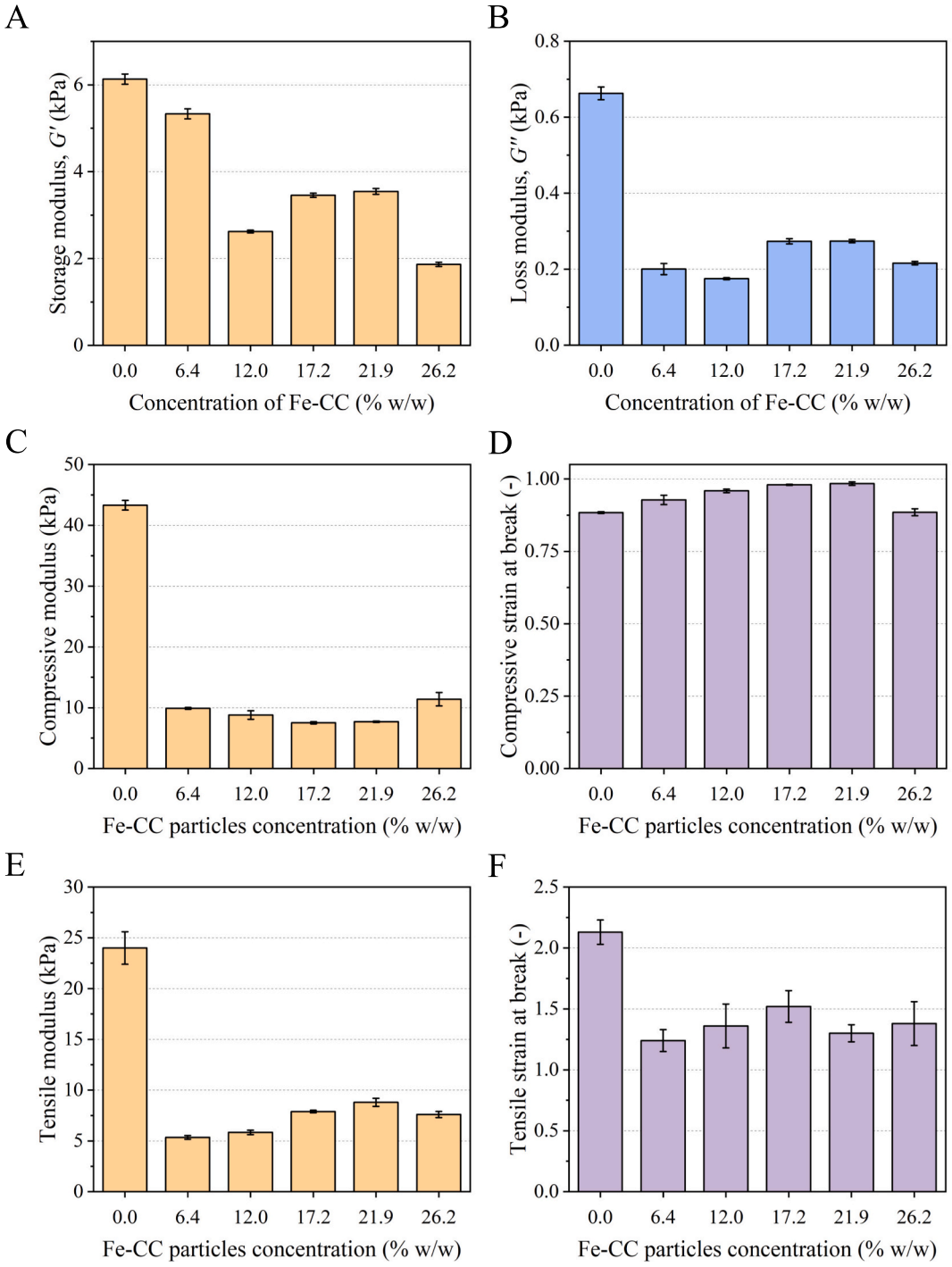

Fig. 3. Mechanical properties of Alginate Mag-SIPNs hydrogels for a fixed amount of accelerant PDMTA (0.11 μmol/g) and iron microparticle (Fe-CC) concentration in the range 0 % to 26.2 % w/w. Storage modulus (A) and loss modulus (B) corresponding to the linear viscoelastic regime for oscillatory shear measurements at increasing strain amplitude and constant frequency of oscillation of 1 Hz. Elastic modulus (C) and strain at break (D) obtained under compressive stress. Elastic modulus (E) and strain at break (F) obtained under tensile stress.

disrupted the polymerization process, thereby affecting the final mechanical properties of the hydrogels.

Alginate Mag-SIPNs hydrogels were also characterized under compressive and tensile stress (refer to curves in Fig. S-4). As observed, when iron microparticles were added to the hydrogel, a considerable decrease in the elastic moduli happened, both under compressive and tensile stress (Figs. 3C and E), indicating a decrease in the stiffness of the materials. Furthermore, two distinct behaviors were observed depending on the stress applied. For the compressive modulus, for particle concentrations of 17.2 and 21.9 % w/w there was a statistically significant minimum (8.42 ± 0.19 kPa and 8.79 ± 0.25 kPa, respectively). The observed increase in compressive modulus upon further increase in particle concentration to 26.2 % is likely attributed to the crowding of particles. This crowding effect should generate a robust resistance against compression, providing a plausible explanation for the observed increase. On the contrary, for measurements under tensile stress, the opposite situation was observed, with the tensile modulus demonstrating a statistically significant maximum (8.8 ± 0.4 kPa) at 21.9 % w/

w particle concentration. Remark also that compressive modulus values were always higher than the modulus values under tensile stress.

Another relevant mechanical parameter is the maximum strain that the hydrogels can withstand before breakage, known as strain at break. For Alginate Mag-SIPNs hydrogels (Figs. 3D and F) two different behaviors were observed depending on the type of applied stress. For measurements under compressive stress (Fig. 3D), there was mainly a slight increase in strain at break with iron microparticle content, with a

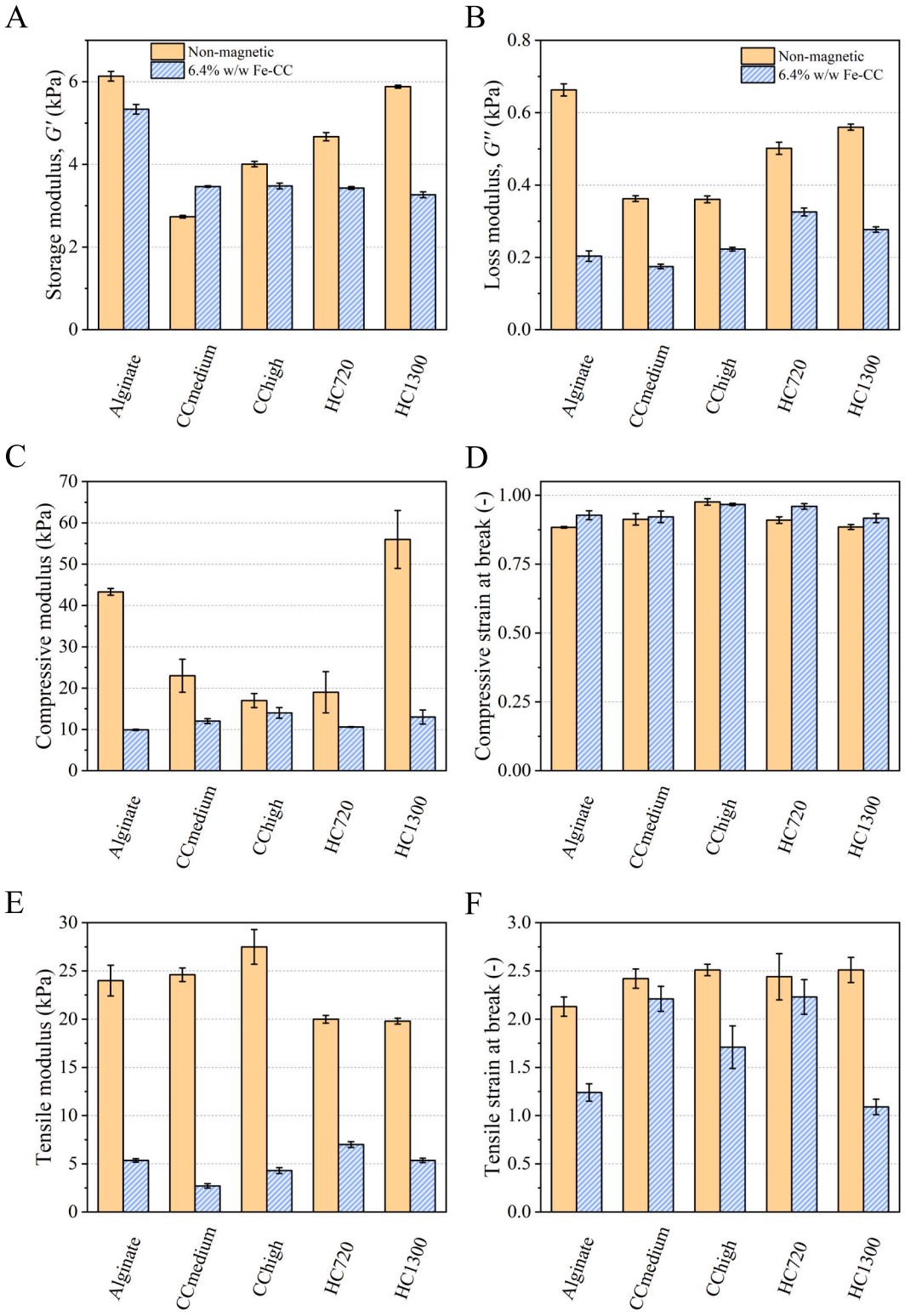

Fig. 4. Mechanical properties of SIPNs hydrogels (non-magnetic and magnetic) based on different linear biopolymers for a fixed amount of accelerant PDMTA (0.11 μmol/g). Storage modulus (A) and loss modulus (B) corresponding to the linear viscoelastic regime for oscillatory shear measurements at increasing strain amplitude and constant frequency of oscillation of 1 Hz. Elastic modulus (C) and strain at break (D) obtained under compressive stress. Elastic modulus (E) and strain at break (F) obtained under tensile stress.

statistically significant maximum for 17.2 and 21.9 % w/w -remark the enormous compressibility of the Mag-SIPNs hydrogels that can be compressed until a maximum of approx. 98 % of their initial height before breakage (Fig. 1C). For measurements under tensile stress the reverse behavior was observed, with a substantial decrease of strain at break (approximately from 210 % to 140 %) when particles were included in the formulation (Fig. 3F), although there were not statistically significant differences between samples containing magnetic microparticles. This difference in behavior when samples were subjected to tensile or compressive stress was likely related to the disruption of the polymer network by the embedded particles, which were expected to provoke "holes" in the polymer network (refer to Section 3.2). Measurements under tensile stress are more sensitive to these defects in the polymer network, whereas under compressive stress the slight enhancements could be due to the iron microparticles opposing to the compression. In the case of hybrid fibrin-agarose hydrogels similar discrepancies were found, with tensile modulus and stress at break under tensile stress decreasing as the agarose content increased, whereas the compressive modulus increased with agarose content [51]. This last result was connected to the high water-holding capacity of agarose.

3.1.3. Mechanical properties of Mag-SIPNs based on different carbohydrate biopolymers

To modulate the mechanical properties of Mag-SIPNs hydrogels even more, alginate was replaced by other carbohydrate biopolymers with different physicochemical properties (please refer to Fig. 1 and Table 1). Considering the results obtained for Alginate Mag-SIPNs hydrogels (Figs. 2 and 3), Mag-SIPNs hydrogels based on other biopolymers were initially synthesized with concentrations of iron microparticles and PMDTA of 6.4 % w/w and 0.11 μmol/g, respectively. In the case of non-magnetic hydrogels, an increase of the storage modulus with the molecular weight of the polymer was observed for systems based on hydroxyl cellulose (HC720 or HC1300), although no statistically significant differences with respect to alginate-based hydrogels were obtained (Figs. 4A and B). For hydrogels based on cellulose charged with carboxyl groups (CCmedium or CChigh) a remarkable decrease of the storage modulus (weakening) was observed with respect to the other non-magnetic hydrogels. In all cases, the storage modulus decreased with the addition of magnetic particles, with the highest value (statistically significant) obtained for Alginate Mag-SIPNs hydrogels, whereas similar values (no statistically significant differences) were obtained for the different cellulose-based Mag-SIPNs hydrogels.

The hydrogels based on different celluloses were also characterized under compressive and tensile stresses (see Fig. 4C to E). For non-magnetic hydrogels, the highest value of the compressive modulus was obtained for the systems based on the polymer HC1300 or alginate, whereas a substantial decrease was observed for the systems based on the other biopolymers (Fig. 4C). A different situation was observed for measurements under tensile stress, with the hydrogels based on alginate, CCmedium and CChigh presenting the highest values of tensile modulus (Fig. 4E). Furthermore, the introduction of magnetic particles resulted in all cases in substantial reductions of the values of the elastic moduli (Fig. 4C and E). For the strain at break, interestingly, no statistically significant differences were observed for the different non-magnetic hydrogels, although slightly higher values were obtained for hydrogels based on cellulose than for hydrogels based on alginate under tensile stress (Fig. 4D and F). The addition of magnetic particles caused no substantial changes in this quantity under compressive stress (Fig. 4D), whereas resulted in a decrease for measurements under tensile stress (Fig. 4F).

To sum up, the mechanical performance of the SIPNs hydrogels (magnetic and non-magnetic) not only depends on the type of biopolymer (alginate, 2-hydroxyethyl cellulose or carboxymethyl cellulose), but also on their mean molecular weight. Furthermore, some general trends were demonstrated regarding the inclusion of magnetic microparticles in the formulation, that make possible to conclude that Mag-SIPNs hydrogels showed smaller values of the storage and elastic moduli (both under tensile and compressive stresses), but maintained a considerable high stretchability and compressibility, as compared with non-magnetic SIPNs hydrogels. This combination of lower elastic moduli with high stretchability and compressibility is ideal for applications that demand maximization of deformation under external stimuli, such as soft robots and actuators with remote control [52].

3.2. Morphological and magnetic characterization of the Mag-SIPNs hydrogels

Mag-SIPNs hydrogels were macroscopically homogeneous, had a soft consistency and were easily manipulated without fracture (Fig. 1B). From the viewpoint of the iron particle distribution, a macroscopic gradient in particle concentration was unavoidable for some Mag-SIPNs hydrogels (Fig. 5A and Fig. S-5). It is interesting to note that Mag-SIPNs hydrogels based on celluloses with a high molecular weight (CChigh and HC1300) did not show appreciable gradient of particle concentration, whereas these based on polymers of low molecular weight (HC720 or alginate) showed a visible gradient of particle concentration. Remark, nevertheless, that not only the molecular weight was important since Mag-SIPNs based on CCmedium (medium molecular weight) showed the highest gradient in magnetic particle concentration.

Scanning electron microscopy (SEM) of Mag-SIPNs hydrogels (Fig. 5B and Fig. S-6) showed the presence of clusters of magnetic particles surrounded by polymeric materials (see for example the area highlighted by a red circle in Fig. 5B). The inclusion of these particles in the hydrogel matrix produced a slight increase in the porosity of the network (Fig. S-7), possibly due to the interference of these particles with the polymerization process and because part of the polymeric material was used to coat the particles and not to form the three-dimensional network. This effect was not observed in the hydrogels that did not contain magnetic particles (Fig. 5C) in which a more homogeneous network and filaments of small sizes were observed.

The swelling behavior of SIPNs hydrogels (non-magnetic and magnetic) was studied by measuring their mass (M_H (t)) over time after immersing them in milli-Q water (Fig. 5). The swelling degree was quantified by the following equation:

$$Q(t) = \frac{M_H(t) - M_H(t=0)}{M_H(t=0)} \quad (1)$$

Differences in swelling degree were observed when using different biopolymers, with hydrogels based on alginate or carboxyl celluloses showing higher water absorption than those based on hydroxyl celluloses, independently of the molecular weight, which did not seem to play any significant role. This should be due to the presence of charges in the hydrogels based on alginate or carboxyl cellulose due to the carboxyl groups, contrarily to hydrogels based on hydroxyl celluloses that are neutral, which make its degree of swelling smaller. Note also that the water absorption was obviously also reflected in the volume of the hydrogels, which notably increased along with mass in these experiments (Fig.S-8). The most relevant result of the swelling experiments was the much greater swelling demonstrated by magnetic hydrogels (Q values up to approx. 28) as compared with not magnetic hydrogels (Q values up to approx. 2) -compare Fig. 5D and E. Moreover, while the water absorption of the non-magnetic hydrogels mainly saturated within the first 24 h, the magnetic hydrogels maintained their ability to absorb water for 48–72 h. An increase of swelling of polymeric hydrogels when particles were included in the network was previously reported by other authors. For example, Bonhome-Espinosa et al. [23] connected the enhancement of the swelling degree of fibrin-based magnetic hydrogels with the formation of particle clusters that served as knots of the polymeric network, resulting in a more opened structure.

The curves of magnetization of Mag-SIPNs hydrogels demonstrated typical ferromagnetic behavior with negligible remanence and coercivity, alike to this of powder of iron microparticles, although with much

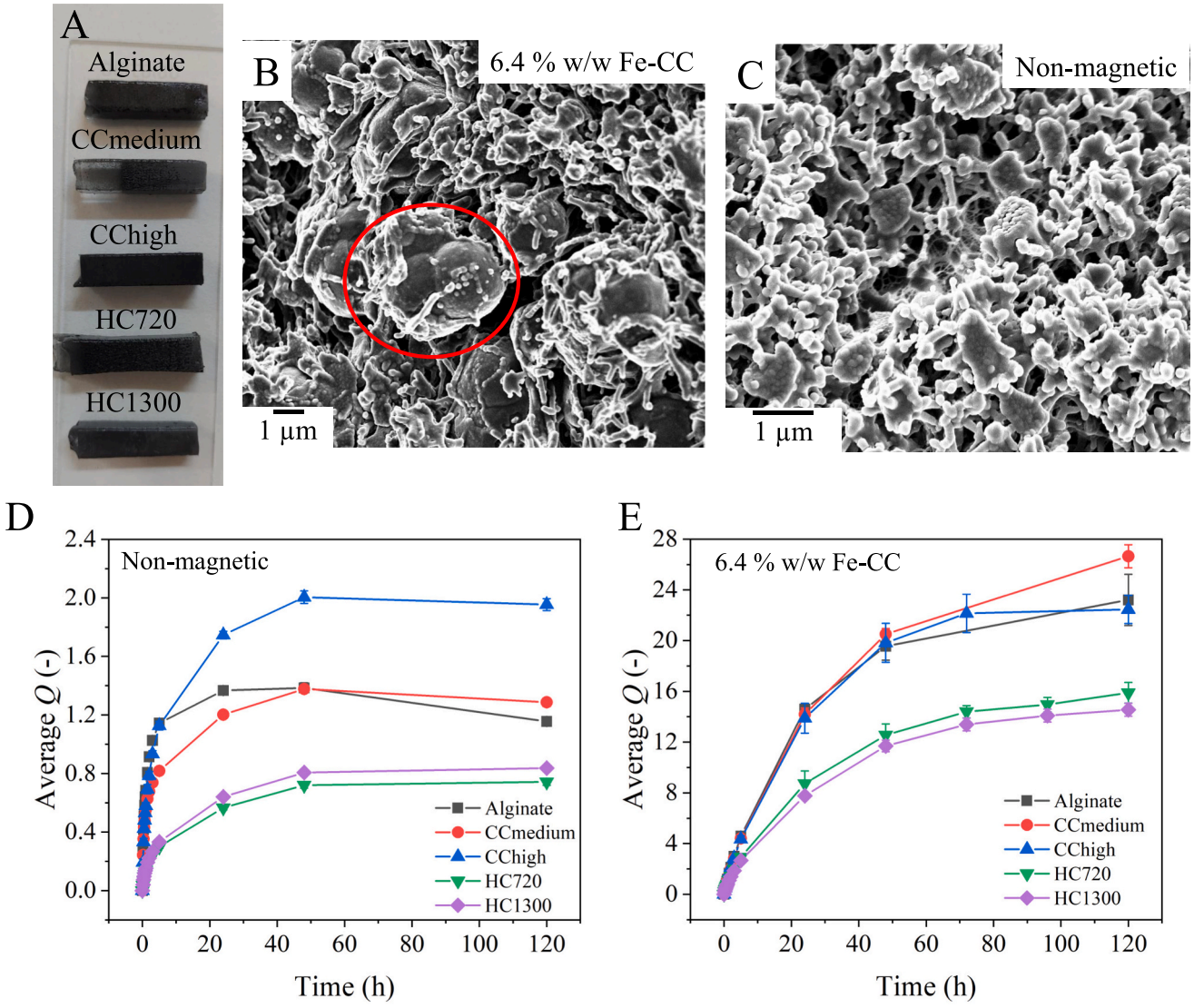

Fig. 5. (A) Mag-SIPNs hydrogels containing 26.4 % w/w concentration of iron microparticles. A particle gradient can be observed in some cases, being more noticeable in CCmedium. (B) and (C) SEM images of the internal structure of HC720, with a concentration of Fe-CC of 6.4 % w/w and without magnetic microparticles, respectively. Note that in (B) a magnetic microparticles have been marked with a red circle. (D) and (E) Swelling behavior as a function of time of immersion in milli-Q water, (D) for non-magnetic SIPNs hydrogels and (E) for Mag-SIPNs hydrogels containing 6.4 % w/w concentration of iron microparticles. (For interpretation of the references to color in this figure legend, the reader is referred to the web version of this article.)

smaller saturation magnetization (Fig. 6A), as expected due to the extensive property of magnetization. When normalized by the saturation magnetization to account for differences in particle concentrations (Fig. 6B), no significant differences among samples themselves or with respect to iron microparticles were observed.

3.3. Magnetic field-induced contraction of the Mag-SIPNs hydrogels

As previously mentioned, one of the main interests of magnetic hydrogels is their application in the field of soft robots and actuators. For these applications, a strong, reversible, and reliable response to the application of a magnetic field is required. Here we evaluated the magnetic responsiveness of the magnetic hydrogels by their compression under the action of a magnetic field gradient generated by a permanent magnet. In these experiments, the different magnetic hydrogels were placed in a reservoir connected laterally to a main canal that was blocked by the hydrogels in the absence of applied magnetic field. For the measurement of the compression of the hydrogels, the magnet was placed close to the hydrogels, which thanks to their strong magnetic character and high compressibility were contracted (see Fig. 6C and D). When the magnet was removed, the magnetic hydrogels tended to return to their natural, more elongated state. For more details about the experimental setup refer to our previous work [10]. In contrast to this previous work, in the present work we used a larger NdFeB magnet which generated a magnetic field that decayed more slowly with the distance from the magnet surface (Fig. S-2) and that, consequently, resulted in larger contractions of the magnetic hydrogels. To maximize the contraction under the action of the applied magnetic field, the hydrogels were placed with their end with lower concentration of particles (when there was appreciable gradient in particle concentration) close to the magnet [53]. We evaluated in this experiment, Mag-SIPNs hydrogels with a concentration of magnetic particles of 26.2 % w/w. For comparison purposes we also evaluated single-network magnetic alginate hydrogels containing the same concentration of magnetic particles, prepared as described in Ref. [10]. It should be noticed that the Mag-SIPNs hydrogels of the present work showed better magneto-mechanical response than the single-network alginate hydrogels, which for the strong magnetic field gradient of the present work showed

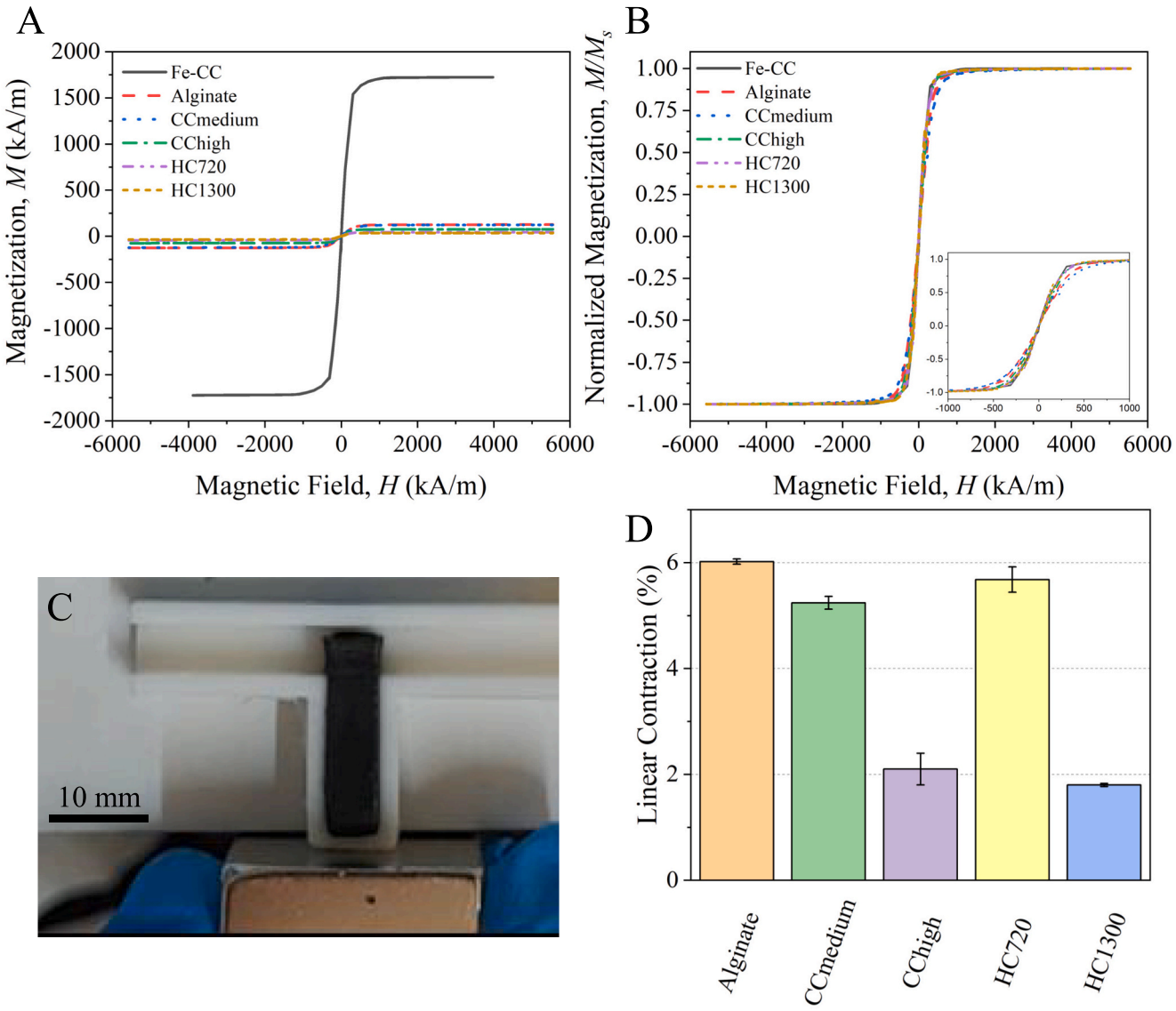

Fig. 6. (A) Magnetization curves of the iron microparticles (Fe-CC) and the different Mag-SIPNs hydrogels. (B) Normalized magnetization curves for comparison purposes. (C) Experimental setup used to measure de deformability of the Mag-SIPNs placed in a reservoir. (D) Linear contraction of the Mag-SIPNs hydrogels under the magnetic field gradient generated by a permanent magnet.

no reversibility of contraction after only one cycle of application/removal of magnetic field (supporting video 1) -remark the stronger magnetic field gradient of the present work at the end of the magnetic hydrogels opposite to the magnet surface, as compared with the one used in Ref. [10] (Fig.S-2). Results demonstrated large values of linear contraction of the Mag-SIPNs hydrogels under application of the magnetic field gradient (Fig. 5C). Furthermore, the Mag-SIPNs hydrogels based on carbohydrate biopolymers of lower molecular weight contracted more in response to the applied magnetic field than the ones based on biopolymers with higher molecular weight. This result agrees with the compressibility characterization (Fig. 4). Finally, it is remarkable that Mag-SIPNs hydrogels demonstrated complete reversibility in their magneto-mechanical response even after 50 cycles of application/removal of magnetic field (supporting video 2).

3.4. Manufacture and testing of a Mag-SIPNs as a magnetic luminescent O_2 sensor

Optical sensors represent an interesting alternative to electrochemical sensors for monitoring biological parameters such as O_2, among others [54]. In contrast to the most common electrochemical sensors, optical sensors are cost-effective and can be read without physical contact [55–57]. But most luminescence oxygen-responsive probes are highly hydrophobic, so over the last few decades, they have been widely encapsulated in synthetic hydrophobic polymers [58–60]. One main problem of these sensors, when they are intended to work in liquid environments, is fixing them to be able to read the luminescent signal from the outside of the liquid container. This problem can be minimized by the incorporation of magnetic particles into the sensing material [59–62]. Within this context, in this section we report, to the best of our knowledge, the first hydrogel luminescent oxygen sensor (based on phosphorescence quenching) fabricated with a natural carbohydrate biopolymer that can be fixed thanks to its strong magnetic response. Since the embedded magnetic microparticles can dramatically affect the optical properties of the hydrogel due to their dark color (filter effect and self-absorption of luminescence emission) [60], we designed and fabricated a disk-like Mag-SIPN hydrogel in which the inner circular region (sensing zone) was free of magnetic microparticles and sensitive to O_2 by quenching of luminescence, and the outer hydrogel ring contained the iron microparticles (magnetic responsive zone) (Fig. 7A). To

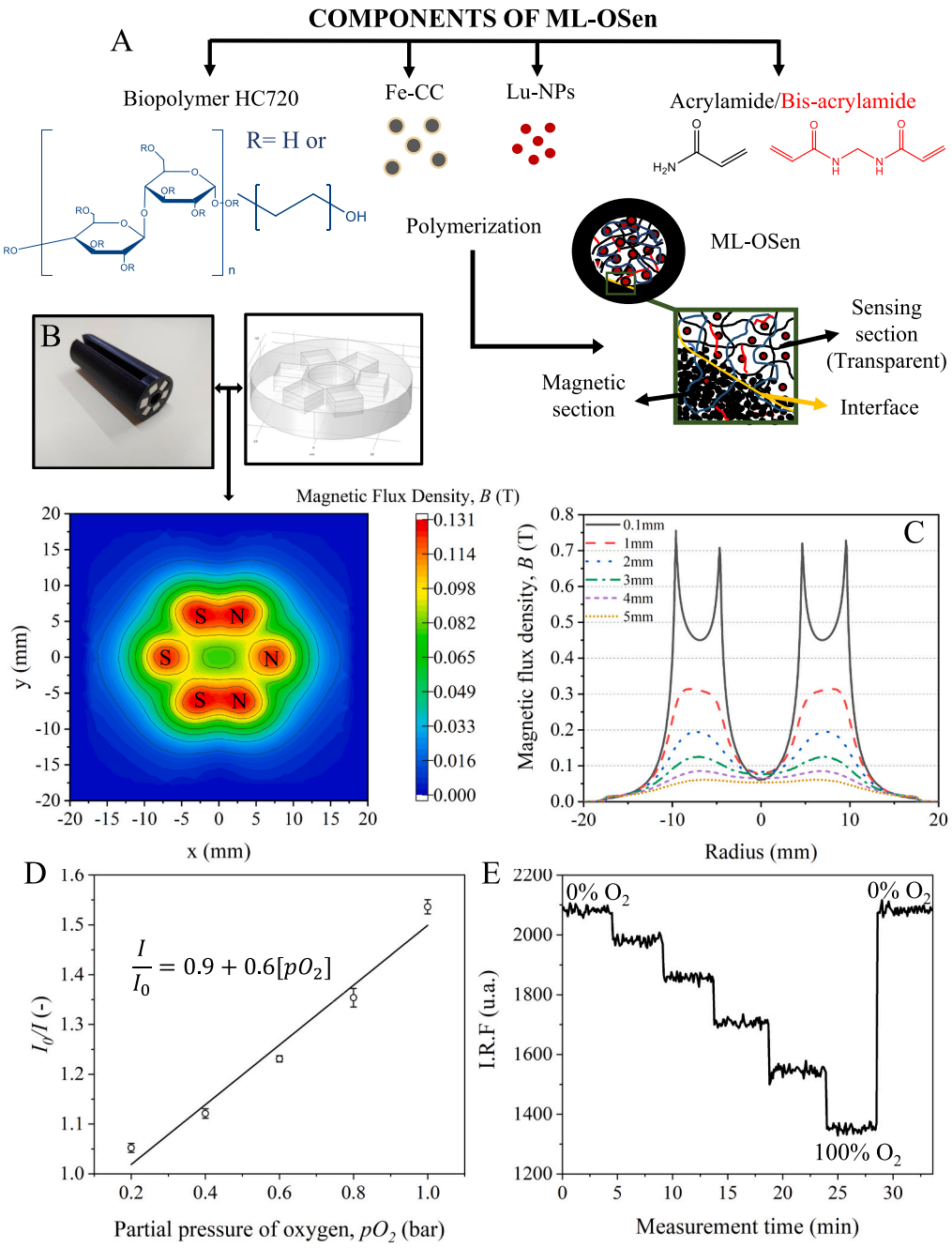

Fig. 7. (A) Composition and structure of the magnetic luminescent O_2 Sensor (ML-Osen). (B) Structure of the magnetic collector, and COMSOL simulation of the resulting magnetic field on a plane 3 mm above the surface of the collector. (C) COMSOL simulation of the resulting magnetic field in a line at different heights above the surface of the collector. (D) Stern-Volmer calibration and (E) relative intensity of fluorescent (I.R.F.) vs. time.

introduce O_2-sensig properties in the inner SIPN hydrogel (sensing zone), O_2-sensitive luminescent nanoparticles (Lu-NPs) (99 ± 7 nm of diameter) were previously prepared by encapsulation of platinum octaethylporphyrin (PtOEP; luminescent O_2 probe; λ_{exc} = 380 nm, λ_{em} = 650 nm) into poly(styrene-*co*-maleic anhydride; 7 % maleic anhydride, M_w = 80,000 Da) by mini-emulsion solvent evaporation [47]. Then, the Lu-NPs were dispersed into the pre-polymerization mixture of the inner SIPN hydrogel (sensing zone).

The hydrophobic nature of Poly(styrene-*co*-maleic anhydride) nanoparticles (Lu-NPs) prevents them from leaking to the aqueous environment. Therefore, the anhydride groups of Lu-NPs (7 %) were previously hydrolyzed in basic media to introduce negative charge (COO^-) on their surface (*Z*-potential of hydrolyzed Lu-NPs was 60.0 ± 0.6 mV). After hydrolysis, the Lu-NPs were easily dispersed into the aqueous pre-polymerization mixture of the inner SIPN (sensing zone). To manufacture the ML-OSen the neutral biopolymer HC720 was selected to avoid aggregation phenomena due to repulsions between negatively charged Lu-NPs and the negatively charges of alginate and carboxymethyl cellulose, besides its mechanical properties and lower swelling degree. Furthermore, for the fabrication of the ML-Osen a higher crosslinker concentration was used for both the non-magnetic SIPN hydrogel circle and the Mag-SIPN hydrogel ring, to avoid an excessive swelling, which could be detrimental to the magnetic and O_2-sensing responses (refer to Section 2.4).

To allow measurements of the oxygen concentration in aqueous solutions from the outside of the liquid container, the fabricated ML-OSen

was fixed by the toroidal magnetic field generated by an array of six block magnets (magnetic collector) placed around the optical fiber probe of 0.5 mm of diameter used for the calibration of the O_2 sensor (Fig. 7B and C) (supporting video 3). To determine the sensitivity and reversibility to oxygen of ML-OSen, the variation of the luminescence intensity of the inner SIPN hydrogel (sensing zone; see Fig. 7) vs. the oxygen concentration was recorded, giving the Stern–Volmer plots [5]. The optical fiber probe was coupled to the homemade magnetic collector and connected to a high-resolution Multi-Led spectrometer. To make measurements with this set-up (see Fig. S-9), the ML-OSen was introduced into a quartz cuvette (1.5 cm thick, 12 cm wide and 10 cm high) containing 100 mL of water. Then, the ML-OSen was attracted and fixed on the wall of the cuvette by the magnetic field generated by the array of magnets, and the luminescence intensity for each O_2 concentration was read. The different O_2 concentrations were established by bubbling into the solution a gas flow with four different percentages of O_2 balanced in N_2. Results of measurements demonstrated an almost linear correlation between the luminescence intensity expressed as the ratio between the intensity in absence of O_2, I_0 and the intensity in presence of O_2, I; I_0/I and the partial pressure of oxygen (pO_2), with a sensitivity to O_2 of $K_{sv} = 0.6$ bar^{-1} (Fig. 7D). The reversibility (Fig. 7E), linear correlation between I_0/I and pO_2, and stability (Fig. S-10) make this proof-of-concept sensor suitable for reliable measurements of the O_2 concentration.

4. Conclusions

In conclusion, we have reported novel magnetic hydrogels consisting of iron microparticles dispersed in semi-interpenetrating polymer networks (SIPNs) based on a cross-linked network and a polymer consisting of five different natural carbohydrate biopolymers. We found that the high mechanical compliance and toughness of the SIPNs made it possible to accommodate a high load of magnetic microparticles without any substantial weakening of the mechanical properties of the resulting magnetic SIPNs (Mag-SIPNs) hydrogels, although a minimum amount of accelerant was needed to minimize particle settling during gelation. The resulting Mag-SIPNs hydrogels demonstrated ideal mechanical properties for smart applications as actuators and sensors with remote control by magnetic field. Specifically, their rather low values of elastic moduli (both under tensile and compressive stresses) and viscoelastic moduli, together with the extremely large values of compressibility and stretchability are optimum for maximizing the magneto-mechanical response of Mag-SIPNs hydrogels under an applied magnetic field. What is more, the presence of magnetic microparticles surprisingly enhanced by an order of magnitude the swelling of the Mag-SIPNs hydrogels, while no dissolution of the polymeric network was observed. We have also reported the compression of the Mag-SIPNs hydrogels under a magnetic field gradient generated by a permanent magnet and observed considerably large values of compression, as well as perfect reversibility during many cycles of application/removal of the magnetic field. This excellent performance and reversibility of the Mag-SIPNs hydrogels paves the way for promising practical applications of these magnetic hydrogels as active parts with remote magnetic control in valve applications for microfluidic or gas devices, or even electromagnetic devices [63–66]. Given the critical relevance of valving and the attractive of precise remote control of valves for disposable biochip applications [67–70], this result is far-reaching in the field of magnetic hydrogel actuators. Finally, we have reported the design and evaluation of a magnetic luminescent oxygen sensor based on the Mag-SPNs hydrogels. Thanks to the strong magnetic character of these hydrogels, this sensor solves the problem of the lack of fixation in the measurement cell, which usually prevents a reliable reading of the optical signal. Considering that oxygen plays a vital role in cellular and enzymatic processes, the real-time monitoring of the O_2 concentration in the internal microenvironment of a natural hydrogel could be crucial [71–74] for monitoring cell and enzymatic bioprocesses. This makes the sensor application of this work even more relevant for future research.

Supplementary data to this article can be found online at https://doi.org/10.1016/j.ijbiomac.2024.129368.

CRediT authorship contribution statement

Alberto Leon-Cecilla: Conceptualization, Formal analysis, Investigation, Validation, Visualization, Writing – original draft. **Cristina Gila-Vilchez:** Conceptualization, Investigation, Validation. **Francisco J. Vazquez-Perez:** Investigation, Validation. **Luis F. Capitan-Vallvey:** Methodology, Resources. **Vanesa Martos:** Funding acquisition, Resources. **María D. Fernandez-Ramos:** Investigation, Methodology, Resources. **Luis Álvarez de Cienfuegos:** Conceptualization, Funding acquisition, Writing – review & editing. **Antonio L. Medina-Castillo:** Conceptualization, Investigation, Methodology, Supervision, Validation, Writing – original draft. **Modesto T. Lopez-Lopez:** Conceptualization, Funding acquisition, Methodology, Project administration, Resources, Supervision, Writing – original draft, Writing – review & editing.

Declaration of competing interest

The authors declare that they have no known competing financial interests or personal relationships that could have appeared to influence the work reported in this paper.

Data availability

The data underlying this study are openly available in Figshare at doi:https://doi.org/10.6084/m9.figshare.24772650.

Acknowledgments

This study was supported by grant PID2020-118498GB-I00 funded by MCIN/AEI/10.13039/501100011033, Spain. A.L.-C. acknowledges grant FPU19/01801 funded by MCIN/AEI/10.13039/501100011033 and "ESF Investing in your future", Spain. V.M. acknowledges VIRTUOUS project, funded by the European Union's Horizon 2020 research and innovation program under the Marie Sklodowska-Curie-RISE Grant Agreement No. 872181 (https://www.virtuoush2020.com/) and the Project European Union's Horizon 2020 research and innovation program under the Marie Sklodowska-Curie-RISE Grant Agreement "SUSTAINABLE" No. 101007702 (https://www.projectsustainable.eu/). A.L.M.-C. acknowledges funding by Plan Propio-Investigación y Transferencia de la Universidad de Granada: "*Programa 9. Proyectos de Investigación para la Incorporación de Jóvenes Doctores a Nuevas Líneas de Investigación en Grupos de la UGR*". Profs. Manuel Toledano and Raquel Osorio are acknowledged for providing access to the universal testing machine Instron 3345. Funding for open access charge: Universidad de Granada/CBUA.

Author statement

We declare that this manuscript is original, has not been published before and is not currently being considered for publication elsewhere.

We confirm that the manuscript has been read and approved by all named authors and that there are no other persons who satisfied the criteria for authorship but are not listed.

We further confirm that the order of authors listed in the manuscript has been approved by all of us.

We understand that the Corresponding Author is the sole contact for the Editorial process.

He is responsible for communicating with the other authors about progress, submissions of revisions and final approval of proofs.

References

[1] F. Castles, S.M. Morris, J.M.C. Hung, M.M. Qasim, A.D. Wright, S. Nosheen, S. S. Choi, B.I. Outram, S.J. Elston, C. Burgess, L. Hill, T.D. Wilkinson, H.J. Coles, Stretchable liquid-crystal blue-phase gels, Nat. Mater. 13 (2014) 817–821, https://doi.org/10.1038/nmat3993.

[2] X. Shi, Z. Deng, P. Zhang, Y. Wang, G. Zhou, L.T. Haan, Wearable optical sensing of strain and humidity: a patterned dual-responsive semi-interpenetrating network of a cholesteric main-chain polymer and a poly(ampholyte), Adv. Funct. Mater. 31 (2021) 2104641, https://doi.org/10.1002/adfm.202104641.

[3] M. López-Valdeolivas, D. Liu, D.J. Broer, C. Sánchez-Somolinos, 4D printed actuators with soft-robotic functions, Macromol. Rapid Commun. 39 (2017) 1700710, https://doi.org/10.1002/marc.201700710.

[4] A. Ryabchun, A. Bobrovsky, Cholesteric liquid crystal materials for tunable diffractive optics, Adv. Opt. Mater. 6 (2018) 1800335, https://doi.org/10.1002/adom.201800335.

[5] A.L. Medina-Castillo, J.F. Fernández-Sánchez, A. Fernández-Gutiérrez, One-step fabrication of multifunctional core-shell fibres by co-electrospinning, Adv. Funct. Mater. 21 (2011) 3488–3495, https://doi.org/10.1002/adfm.201100707.

[6] Y. Zhang, Q. Fu, J. Ge, Photonic sensing of organic solvents through geometric study of dynamic reflection spectrum, Nat. Commun. 6 (2015), https://doi.org/10.1038/ncomms8510.

[7] L. Tang, L. Wang, X. Yang, Y. Feng, Y. Li, W. Feng, Poly(N-isopropylacrylamide)-based smart hydrogels: design, properties and applications, Prog. Mater. Sci. 115 (2021) 100702, https://doi.org/10.1016/j.pmatsci.2020.100702.

[8] X. Li, X. Su, Multifunctional smart hydrogels: potential in tissue engineering and cancer therapy, J. Mater. Chem. B 6 (2018) 4714–4730, https://doi.org/10.1039/c8tb01078a.

[9] H.-W. Huang, M.S. Sakar, A.J. Petruska, S. Pané, B.J. Nelson, Soft micromachines with programmable motility and morphology, Nat. Commun. 7 (2016), https://doi.org/10.1038/ncomms12263.

[10] F.J. Vazquez-Perez, C. Gila-Vilchez, J.D.G. Duran, A. Zubarev, L.A. de Cienfuegos, L. Rodriguez-Arco, M.T. Lopez-Lopez, Composite polymer hydrogels with high and reversible elongation under magnetic stimuli, Polymer (Guildf). 230 (2021) 124093, https://doi.org/10.1016/j.polymer.2021.124093.

[11] S.R. Goudu, I.C. Yasa, X. Hu, H. Ceylan, W. Hu, M. Sitti, Biodegradable untethered magnetic hydrogel Milli-grippers, Adv. Funct. Mater. 30 (2020) 2004975, https://doi.org/10.1002/adfm.202004975.

[12] Y. Wu, X. Dong, J. Kim, C. Wang, M. Sitti, Wireless soft millirobots for climbing three-dimensional surfaces in confined spaces, Sci. Adv. 8 (2022), https://doi.org/10.1126/sciadv.abn3431.

[13] X. Chen, C. Tian, H. Zhang, H. Xie, Biodegradable magnetic hydrogel robot with multimodal locomotion for targeted cargo delivery, ACS Appl. Mater. Interf. 15 (2023) 28922–28932, https://doi.org/10.1021/acsami.3c02703.

[14] L. Mei, J. Cong, S. Li, T. Ren, Y. Bai, Q. Liu, C. Miao, W. Ding, T. Luo, Polyacrylamide-chitosan based magnetic hydrogels with high stiffness and ultra-toughness, Compos. Part A Appl. Sci. Manuf. 168 (2023) 107478, https://doi.org/10.1016/j.compositesa.2023.107478.

[15] C. Gila-Vilchez, J.D.G. Duran, F. Gonzalez-Caballero, A. Zubarev, M.T. Lopez-Lopez, Magnetorheology of alginate ferrogels, Smart Mater. Struct. 28 (2019) 35018, https://doi.org/10.1088/1361-665x/aafeac.

[16] M.C. Mañas-Torres, C. Gila-Vilchez, F.J. Vazquez-Perez, P. Kuzhir, D. Momier, J.-C. Scimeca, A. Borderie, M. Goracci, F. Burel-Vandenbos, C. Blanco-Elices, I. A. Rodriguez, M. Alaminos, L.Á. de Cienfuegos, M.T. Lopez-Lopez, Injectable magnetic-responsive short-peptide supramolecular hydrogels: ex vivo and in vivo evaluation, ACS Appl. Mater. & Interf. 13 (2021) 49692–49704, https://doi.org/10.1021/acsami.1c13972.

[17] R. Contreras-Montoya, A.B. Bonhome-Espinosa, A. Orte, D. Miguel, J.M. Delgado-López, J.D.G. Duran, J.M. Cuerva, M.T. Lopez-Lopez, L.Á. De Cienfuegos, Iron nanoparticles-based supramolecular hydrogels to originate anisotropic hybrid materials with enhanced mechanical strength, Mater. Chem Front. 2 (2018) 686–699, https://doi.org/10.1039/c7qm00573c.

[18] R. Singh, B. Datta, Advances in biomedical and environmental applications of magnetic hydrogels, ACS Appl. Polym. Mater. 5 (2023) 5474–5494, https://doi.org/10.1021/acsapm.3c00815.

[19] Z. Chen, S. Song, J. Ma, S. Da Ling, Y.D. Wang, T.T. Kong, J.H. Xu, Fabrication of magnetic core/shell hydrogels via microfluidics for controlled drug delivery, Chem. Eng. Sci. 248 (2022) 117216, https://doi.org/10.1016/j.ces.2021.117216.

[20] Y. He, J. Tang, Y. Hu, S. Yang, F. Xu, M. Zrínyi, Y. Mei Chen, Magnetic hydrogel-based flexible actuators: a comprehensive review on design, properties, and applications, Chem. Eng. J. 462 (2023) 142193, https://doi.org/10.1016/j.cej.2023.142193.

[21] Y. Li, C.T. Poon, M. Li, T.J. Lu, B. Pingguan-Murphy, F. Xu, Chinese-noodle-inspired muscle myofiber fabrication, Adv. Funct. Mater. 25 (2015) 5999–6008, https://doi.org/10.1002/adfm.201502018.

[22] M. Barczak, P. Borowski, C. Gila-Vilchez, M. Alaminos, F. González-Caballero, M. T. López-López, Revealing importance of particles' surface functionalization on the properties of magnetic alginate hydrogels, Carbohydr. Polym. 247 (2020) 116747, https://doi.org/10.1016/j.carbpol.2020.116747.

[23] A.B. Bonhome-Espinosa, F. Campos, I.A. Rodriguez, V. Carriel, J.A. Marins, A. Zubarev, J.D.G. Duran, M.T. Lopez-Lopez, Effect of particle concentration on the microstructural and macromechanical properties of biocompatible magnetic hydrogels, Soft Matter 13 (2017) 2928–2941, https://doi.org/10.1039/c7sm00388a.

[24] A. Leon-Cecilla, F.J. Vazquez-Perez, C. Gila-Vilchez, L. Álvarez de Cienfuegos, M. T. Lopez-Lopez, Alginate hydrogels reinforced by dehydration under stress—application to a soft magnetic actuator, Gels 9 (2023) 39, https://doi.org/10.3390/gels9010039.

[25] E.S. Dragan, Design and applications of interpenetrating polymer network hydrogels. A review, Chem. Eng. J. 243 (2014) 572–590, https://doi.org/10.1016/j.cej.2014.01.065.

[26] Y. He, Y. Li, Y. Sun, S. Zhao, M. Feng, G. Xu, H. Zhu, P. Ji, H. Mao, Y. He, Z. Gu, A double-network polysaccharide-based composite hydrogel for skin wound healing, Carbohydr. Polym. 261 (2021) 117870, https://doi.org/10.1016/j.carbpol.2021.117870.

[27] L. Li, P. Wu, F. Yu, J. Ma, Double network hydrogels for energy/environmental applications: challenges and opportunities, J. Mater. Chem. A Mater. 10 (2022) 9215–9247, https://doi.org/10.1039/D2TA00540A.

[28] H. Huang, Z. Dong, X. Ren, B. Jia, G. Li, S. Zhou, X. Zhao, W. Wang, High-strength hydrogels: fabrication, reinforcement mechanisms, and applications, Nano Res. 16 (2023) 3475–3515, https://doi.org/10.1007/s12274-022-5129-1.

[29] V. Gold (Ed.), The IUPAC Compendium of Chemical Terminology, International Union of Pure and Applied Chemistry (IUPAC), 2019, https://doi.org/10.1351/goldbook.

[30] X. Liu, Y. Yang, M.E. Inda, S. Lin, J. Wu, Y. Kim, X. Chen, D. Ma, T.K. Lu, X. Zhao, Magnetic living hydrogels for intestinal localization, retention, and diagnosis, Adv. Funct. Mater. 31 (2021) 2010918, https://doi.org/10.1002/adfm.202010918.

[31] R.E. Webber, C. Creton, H.R. Brown, J.P. Gong, Large strain hysteresis and Mullins effect of tough double-network hydrogels, Macromolecules 40 (2007) 2919–2927, https://doi.org/10.1021/ma062924y.

[32] Y.-H. Na, Y. Tanaka, Y. Kawauchi, H. Furukawa, T. Sumiyoshi, J.P. Gong, Y. Osada, Necking phenomenon of double-network gels, Macromolecules 39 (2006) 4641–4645, https://doi.org/10.1021/ma060568d.

[33] J.P. Gong, Why are double network hydrogels so tough? Soft Matter 6 (2010) 2583, https://doi.org/10.1039/b924290b.

[34] Y. Chen, L. Chen, B. Geng, F. Chen, Y. Yuan, D. Li, Y.-X. Wang, W. Jia, W. Hu, Triple-network-based conductive polymer hydrogel for soft and elastic bioelectronic interfaces, SmartMat (2023), https://doi.org/10.1002/smm2.1229.

[35] F. Li, X. Cai, G. Liu, H. Xu, W. Chen, Piezoionic SnSe nanosheets-double network hydrogel for self-powered strain sensing and energy harvesting, Adv. Funct. Mater. (2023), https://doi.org/10.1002/adfm.202300701.

[36] T. Liu, W. Chen, K. Li, S. Long, X. Li, Y. Huang, Toughening weak polyampholyte hydrogels with weak chain entanglements via a secondary equilibrium approach, Polymers (Basel) 15 (2023) 2644, https://doi.org/10.3390/polym15122644.

[37] T. Matsuda, R. Kawakami, R. Namba, T. Nakajima, J.P. Gong, Mechanoresponsive self-growing hydrogels inspired by muscle training, Science 363 (2019) (1979) 504–508, https://doi.org/10.1126/science.aau9533.

[38] Y. Huang, S. Qian, J. Zhou, W. Chen, T. Liu, S. Yang, S. Long, X. Li, Achieving swollen yet strengthened hydrogels by reorganizing multiphase network structure, Adv. Funct. Mater. 33 (2023), https://doi.org/10.1002/adfm.202213549.

[39] M.-K. Zhang, X.-H. Zhang, G.-Z. Han, Magnetic alginate/PVA hydrogel microspheres with selective adsorption performance for aromatic compounds, Sep. Purif. Technol. 278 (2021) 119547, https://doi.org/10.1016/j.seppur.2021.119547.

[40] M.-K. Zhang, X.-H. Ling, X.-H. Zhang, G.-Z. Han, A novel alginate/PVA hydrogel -supported Fe3O4 particles for efficient heterogeneous Fenton degradation of organic dyes, Colloids Surf. A Physicochem. Eng. Asp. 652 (2022) 129830, https://doi.org/10.1016/j.colsurfa.2022.129830.

[41] T. Wan, J. Wang, S. He, T. Wang, Y. Zheng, F. Xie, Q. Tang, Synthesis and lead ion absorption of magnetic hydrogel nanocomposite absorbents with semi-IPNs structure, Polym. Bull. 80 (2023) 3633–3647, https://doi.org/10.1007/s00289-022-04220-3.

[42] A. Roy, Z. Zhang, M.K. Eiken, A. Shi, A. Pena-Francesch, C. Loebel, Programmable tissue folding patterns in structured hydrogels, Adv. Mater. (2023), https://doi.org/10.1002/adma.202300017.

[43] S. Mandal, S. Kumari, M. Kumar, U. Ojha, Supplementary Networking of Interpenetrating Polymer System (SNIPSy) strategy to develop strong & high water content ionic hydrogels for solid electrolyte applications, Adv. Funct. Mater. 31 (2021) 2100251, https://doi.org/10.1002/adfm.202100251.

[44] J. Spangenberg, D. Kilian, C. Czichy, T. Ahlfeld, A. Lode, S. Günther, S. Odenbach, M. Gelinsky, Bioprinting of magnetically deformable scaffolds, ACS Biomater. Sci. Eng. 7 (2021) 648–662, https://doi.org/10.1021/acsbiomaterials.0c01371.

[45] I. Donati, A. Gamini, G. Skjåk-Bræk, A. Vetere, C. Campa, A. Coslovi, S. Paoletti, Determination of the diadic composition of alginate by means of circular dichroism: a fast and accurate improved method, Carbohydr. Res. 338 (2003) 1139–1142, https://doi.org/10.1016/S0008-6215(03)00094-6.

[46] E.R. Morris, D.A. Rees, D. Thom, Characterisation of alginate composition and block-structure by circular dichroism, Carbohydr. Res. 81 (1980) 305–314, https://doi.org/10.1016/S0008-6215(00)85661-X.

[47] G. Mistlberger, A.L. Medina-Castillo, S.M. Borisov, T. Mayr, A. Fernández-Gutiérrez, J.F. Fernandez-Sanchez, I. Klimant, Mini-emulsion solvent evaporation: a simple and versatile way to magnetic nanosensors, Microchim. Acta 172 (2010) 299–308, https://doi.org/10.1007/s00604-010-0492-0.

[48] H. Haider, C.H. Yang, W.J. Zheng, J.H. Yang, M.X. Wang, S. Yang, M. Zrínyi, Y. Osada, Z. Suo, Q. Zhang, J. Zhou, Y.M. Chen, Exceptionally tough and notch-insensitive magnetic hydrogels, Soft Matter 11 (2015) 8253–8261, https://doi.org/10.1039/c5sm01487e.

[49] H.H. Winter, Can the gel point of a cross-linking polymer be detected by the G′-G″ crossover? Polym. Eng. Sci. 27 (1987) 1698–1702, https://doi.org/10.1002/pen.760272209.

[50] F. Chambon, H.H. Winter, Linear viscoelasticity at the gel point of a crosslinking PDMS with imbalanced stoichiometry, J. Rheol. (N Y N Y). 31 (1987) 683–697, https://doi.org/10.1122/1.549955.
[51] G. Scionti, M. Moral, M. Toledano, R. Osorio, J.D.G. Durán, M. Alaminos, A. Campos, M.T. López-López, Effect of the hydration on the biomechanical properties in a fibrin-agarose tissue-like model, J. Biomed. Mater. Res. A 102 (2014) 2573–2582, https://doi.org/10.1002/jbm.a.34929.
[52] X. Liu, J. Liu, S. Lin, X. Zhao, Hydrogel machines, Mater. Today 36 (2020) 102–124, https://doi.org/10.1016/j.mattod.2019.12.026.
[53] X. Zhao, J. Kim, C.A. Cezar, N. Huebsch, K. Lee, K. Bouhadir, D.J. Mooney, Active scaffolds for on-demand drug and cell delivery, Proc. Natl. Acad. Sci. 108 (2011) 67–72, https://doi.org/10.1073/pnas.1007862108.
[54] R. Narayanaswamy, O.S. Wolfbeis, Optical Sensors, Springer Berlin Heidelberg, 2004, https://doi.org/10.1007/978-3-662-09111-1.
[55] C. McDonagh, C.S. Burke, B.D. MacCraith, Optical chemical sensors, Chem. Rev. 108 (2008) 400–422, https://doi.org/10.1021/cr068102g.
[56] O. Wolfbeis, Biosensors CRC Press: Boca Raton, FL, 1991.
[57] G. Orellana, M.C. Moreno-Bondi (Eds.), Frontiers in Chemical Sensors, Springer-Verlag, 2005, https://doi.org/10.1007/3-540-27757-9.
[58] J. Choi, D.-M. Shin, H. Song, D. Lee, K. Kim, Current achievements of nanoparticle applications in developing optical sensing and imaging techniques, Nano Converg. 3 (2016), https://doi.org/10.1186/s40580-016-0090-x.
[59] G. Mistlberger, S.M. Borisov, I. Klimant, Enhancing performance in optical sensing with magnetic nanoparticles, Sensors Actuators B Chem. 139 (2009) 174–180, https://doi.org/10.1016/j.snb.2008.11.008.
[60] A.L. Medina-Castillo, G. Mistlberger, J.F. Fernandez-Sanchez, A. Segura-Carretero, I. Klimant, A. Fernandez-Gutierrez, Novel strategy to design magnetic, molecular imprinted polymers with well-controlled structure for the application in optical sensors, Macromolecules 43 (2009) 55–61, https://doi.org/10.1021/ma902095s.
[61] P. Chojnacki, G. Mistlberger, I. Klimant, Separable magnetic sensors for the optical determination of oxygen, Angew. Chem. 119 (2007) 9006–9009, https://doi.org/10.1002/ange.200702068.
[62] G. Mistlberger, P. Chojnacki, I. Klimant, Magnetic sensor particles: an optimized magnetic separator with an optical window, J. Phys. D. Appl. Phys. 41 (2008) 85003, https://doi.org/10.1088/0022-3727/41/8/085003.
[63] Y. Wang, K. Toyoda, K. Uesugi, K. Morishima, A simple micro check valve using a photo-patterned hydrogel valve core, Sens. Actuators A Phys. 304 (2020) 111878, https://doi.org/10.1016/j.sna.2020.111878.
[64] S. Haefner, R. Koerbitz, P. Frank, M. Elstner, A. Richter, High integration of microfluidic circuits based on hydrogel valves for MEMS control, Adv. Mater. Technol. 3 (2018) 1700108, https://doi.org/10.1002/admt.201700108.
[65] H. Mazaheri, A. Namdar, A. Amiri, Behavior of a smart one-way micro-valve considering fluid–structure interaction, J. Intell. Mater. Syst. Struct. 29 (2018) 3960–3971, https://doi.org/10.1177/1045389X18803445.
[66] H. Lin, J. Tan, J. Zhu, S. Lin, Y. Zhao, W. Yu, H. Hojaiji, B. Wang, S. Yang, X. Cheng, Z. Wang, E. Tang, C. Yeung, S. Emaminejad, A programmable epidermal microfluidic valving system for wearable biofluid management and contextual biomarker analysis, Nat. Commun. 11 (2020) 4405, https://doi.org/10.1038/s41467-020-18238-6.
[67] C. Lu, Y. Xie, Y. Yang, M.M.-C. Cheng, C.-G. Koh, Y. Bai, L.J. Lee, Y.-J. Juang, New valve and bonding designs for microfluidic biochips containing proteins, Anal. Chem. 79 (2006) 994–1001, https://doi.org/10.1021/ac0615798.
[68] R. Mohan, B.R. Schudel, A.V. Desai, J.D. Yearsley, C.A. Apblett, P.J.A. Kenis, Design considerations for elastomeric normally closed microfluidic valves, Sensors Actuators B Chem. 160 (2011) 1216–1223, https://doi.org/10.1016/j.snb.2011.09.051.
[69] K.W. Oh, C.H. Ahn, A review of microvalves, J. Micromech. Microeng. 16 (2006) R13–R39, https://doi.org/10.1088/0960-1317/16/5/r01.
[70] G.T. Kovacs, Micromachined Transducers Sourcebook, McGraw-Hill, New York, 1998.
[71] Y.-E.L. Koo, Y. Cao, R. Kopelman, S.M. Koo, M. Brasuel, M.A. Philbert, Real-time measurements of dissolved oxygen inside live cells by organically modified silicate fluorescent nanosensors, Anal. Chem. 76 (2004) 2498–2505, https://doi.org/10.1021/ac035493f.
[72] A. Bigdeli, F. Ghasemi, H. Golmohammadi, S. Abbasi-Moayed, M.A.F. Nejad, N. Fahimi-Kashani, S. Jafarinejad, M. Shahrajabian, M.R. Hormozi-Nezhad, Nanoparticle-based optical sensor arrays, Nanoscale 9 (2017) 16546–16563, https://doi.org/10.1039/c7nr03311g.
[73] H. Xu, J.W. Aylott, R. Kopelman, T.J. Miller, M.A. Philbert, A real-time ratiometric method for the determination of molecular oxygen inside living cells using sol-gel-based spherical optical nanosensors with applications to rat C6 glioma, Anal. Chem. 73 (2001) 4124–4133, https://doi.org/10.1021/ac0102718.
[74] S.M. Borisov, O.S. Wolfbeis, Optical Biosensors, Chem. Rev. 108 (2008) 423–461, https://doi.org/10.1021/cr068105t.